

Frequency-tunable single-photon router based on a microresonator containing a driven three-level emitter

Jin-Song Huang(黄劲松), Jing-Lan Hu(胡菁兰), Yan-Ling Li(李艳玲), and Zhong-Hui Xu(徐中辉)

Citation: Chin. Phys. B, 2024, 33 (**6**): 064202. DOI: 10.1088/1674-1056/ad362a
Journal homepage: http://cpb.iphy.ac.cn; http://iopscience.iop.org/cpb

What follows is a list of articles you may be interested in

Bidirectional highly-efficient quantum routing in a T-bulge-shaped waveguide

Jia-Hao Zhang(张家豪), Da-Yong He(何大永), Gang-Yin Luo(罗刚银), Bi-Dou Wang(王弼陡), and Jin-Song Huang(黄劲松)
Chin. Phys. B, 2021, 30 (**3**): 034204. DOI: 10.1088/1674-1056/abd38c

Far-zone behaviors of scattering-induced statistical properties of partially polarized spatially and spectrally partially coherent electromagnetic pulsed beam

Yan Li(李艳), Ming Gao(高明)†, Hong Lv(吕宏), Li-Guo Wang(王利国), and Shen-He Ren(任神河)
Chin. Phys. B, 2020, 29 (**10**): 104201. DOI: 10.1088/1674-1056/ab9de7

Gain-induced large optical torque in optical twist settings

Genyan Li(李艮艳), Xiao Li(李肖), Lei Zhang(张磊), Jun Chen(陈君)
Chin. Phys. B, 2020, 29 (**8**): 084201. DOI: 10.1088/1674-1056/ab9616

Experimental determination of distributions of soot particle diameter and number density by emission and scattering techniques

Huawei Liu(柳华蔚), Shu Zheng(郑树)
Chin. Phys. B, 2019, 28 (**1**): 014206. DOI: 10.1088/1674-1056/28/1/014206

Single-photon scattering by two separated atoms in a supercavity

Wei Zhu(朱伟), Xiao Xiao(肖骁), Duan-Lu Zhou(周端陆), Peng Zhang(张芃)
Chin. Phys. B, 2016, 25 (**6**): 064203. DOI: 10.1088/1674-1056/25/6/064203

Frequency-tunable single-photon router based on a microresonator containing a driven three-level emitter

Jin-Song Huang(黄劲松)[1,†], Jing-Lan Hu(胡菁兰)[1], Yan-Ling Li(李艳玲)[1], and Zhong-Hui Xu(徐中辉)[2]

[1] *School of Information Engineering, Jiangxi University of Science and Technology, Ganzhou* 341000, *China*
[2] *Faculty of Science, Jiangxi University of Science and Technology, Ganzhou* 341000, *China*

(Received 31 December 2023; revised manuscript received 11 March 2024; accepted manuscript online 21 March 2024)

We propose a frequency-tunable router of single photons with high routing efficiency, which is constructed by two waveguides mediately linked by a single-mode whispering gallery resonator with a driven three-level emitter. Quantum routing probability in the output port is obtained via the real-space Hamiltonian. By adjusting the resonator–emitter coupling and the drive, the desired continuous central frequencies for the resonance peaks of routing photons can be manipulated nearly linearly, with the assistance of Rabi splitting effect and optical Stark shift. The proposed routing system may provide potential applications in designing other frequency-modulation quantum optical devices, such as multiplexers, filters, and so on.

Keywords: quantum routing, scattering theory, optical waveguide, microresonator

PACS: 42.50.Ex, 03.65.Nk, 42.79.Gn, 42.60.Da **DOI:** 10.1088/1674-1056/ad362a

1. Introduction

In a quantum network, the router is a very core component for distributing quantum information.[1] In optical quantum routing systems, one-dimensional optical waveguides are used as quantum channels, and photons are transmitted as carriers in different channels through waveguide quantum electrodynamics (wQED),[2] which can effectively control the transmission of photons by tailoring the couplings between photon fields and quantum emitters. Consequently, a wide variety of studies on quantum routing are implemented in various wQED systems, including atomic qubits,[3–7] superconducting qubits,[8–12] quantum dots,[13,14] optomechanical systems,[15,16] optical cavity systems,[17–20] and chiral waveguide systems.[21–25]

Generally, for an optical transmission system the incident frequency should match the resonance frequency of the coupled emitter in the router, which enables the router work efficiently. Off-resonance photons do not function greatly since there are no couplings with the quantum emitter. However, some targeted off-resonance signals may be desired for the port users, which may restrict their extensive applications of these routing devices. Thus, there is considerable interest to design a quantum router capable of transmitting some selectable frequencies on demand for the input light signals. One feasible way to address the problem is to adopt the frequency-modulation technology to match the targeted frequencies with good tuning controllability, which has been applied in tunable frequency optical combs,[26,27] single-photon diode,[28] and tunable bandpass filters.[29–35]

Motivated by these considerations, we propose a novel frequency-tunable router of single photons based on a double-waveguide structure connected by a whispering-gallery-mode resonator with a driven three-level system. To the best of our knowledge, few studies on frequency-tunable routing for single photons have been carried out. Compared with our previous scheme,[36] where the bandpass router is constructed by a T-shaped waveguide linked by a driven three-level emitter, and a reflector with the accurate phase shift is utilized to improve the routing efficiency, the proposed routing structure only consists of a single-point resonator coupled with a driven three-level emitter, and there is not the additional reflecting mirror, which reduces its complexity of the coupled structure. By using a real-space approach, the single-photon routing amplitude from the bus waveguide to another is obtained analytically. By varying the resonator–emitter coupling and the drive, the continuously resonance frequencies for the routing peaks of single photons can shift almost linearly away from the fixed resonance frequency of the microresonator, under the joint effects of Rabi splitting and optical Stark shift, which indicates that the tunable routing can be achieved effectively.

2. Theoretical model

The schematic diagram is shown in Fig. 1, where we consider two quantum channels constructed by one bus waveguide a and another drop waveguide b. These two waveguides interact with the counter clockwise mode of a whispering gallery resonator. Likewise, a driven three-level emitter, characterized by the ground state $|g\rangle$, the excited state $|e\rangle$ and the metastable state $|s\rangle$, is also coupled to the single-mode resonator through the transition $|g\rangle \leftrightarrow |e\rangle$, while another transition $|s\rangle \leftrightarrow |e\rangle$ is

[†]Corresponding author. E-mail: jshuangjs@126.com

© 2024 Chinese Physical Society and IOP Publishing Ltd

performed by a classical driving field with Rabi frequency Ω. When a single photon is launched into the bus waveguide, the propagating photon will move forward or is routed to the drop port with the help of the coupled emitter, under the mode-matching condition of the resonator mode and the guided-wave mode.

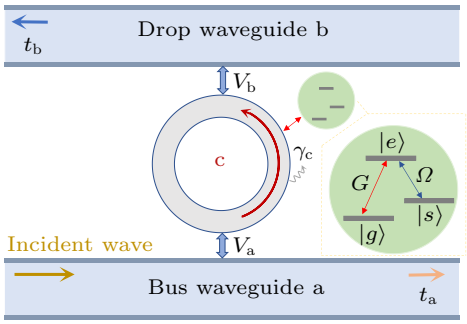


Fig. 1. Schematic view of a single-photon router made of two one-dimensional waveguides coupled to a single-mode whispering gallery resonator with a driven three-level system. A single photon is incident from the left side of the bus waveguide a, and can be routed to the drop waveguide b by the coupled resonator.

Under the linear dispersions of two guided-wave modes and the rotating wave approximation, the Hamiltonian in real space[37,38] for the coupled system can be expressed as ($\hbar = 1$)

$$\begin{aligned} H =& \int \mathrm{d}x \left[-\mathrm{i}\upsilon_g C^\dagger_{\mathrm{Ra}}(x)\frac{\partial C_{\mathrm{Ra}}(x)}{\partial x} + \mathrm{i}\upsilon_g C^\dagger_{\mathrm{Lb}}(x)\frac{\partial C_{\mathrm{Lb}}(x)}{\partial x}\right] \\ &+ V_a \int \mathrm{d}x\delta(x)[C_{\mathrm{Ra}}(x)c^\dagger + C^\dagger_{\mathrm{Ra}}(x)c] \\ &+ V_b \int \mathrm{d}x\delta(x)[C_{\mathrm{Lb}}(x)c^\dagger + C^\dagger_{\mathrm{Lb}}(x)c] \\ &+ (\omega_c - \mathrm{i}\gamma_c)c^\dagger c + (\omega_e - \mathrm{i}\gamma_e)|e\rangle\langle e| + (\omega_s - \mathrm{i}\gamma_s)|s\rangle\langle s| \\ &+ \Omega(|e\rangle\langle s| + |s\rangle\langle e|) + G(c^\dagger|g\rangle\langle e| + c|e\rangle\langle g|). \end{aligned} \tag{1}$$

Here, we focus on the single resonator-mode case in the weak coupling regime, while the mode splitting for the single-mode resonator from the scattered quantum emitter is not taken into account in the strong coupling regime. The ground state level has been considered as the energy reference. υ_g is the group velocity of the propagating photon. $C^\dagger_{\mathrm{Ra}}(x)$ and $C^\dagger_{\mathrm{Lb}}(x)$ denote creating a right-traveling (left-traveling) photon in the waveguide a and waveguide b, respectively. ω_c, ω_e, and ω_s are the transition frequencies of the resonator and two high energy-level states of the emitter, respectively. γ_c, γ_e, and γ_s describe the intrinsic loss rates of the resonator and these two states, respectively. $V_{a(b)}$ denotes the coupling strength between the resonator and the bus (drop) waveguide, while G is the coupling strength between the resonator and the three-level system.

Assume that the light signal with the energy $\omega = \upsilon_g k$ enters from the left port of the bus waveguide, and the three-level emitter is initially in the ground state, then the scattering eigenstate of the Hamiltonian (1) is

$$\begin{aligned} |\psi\rangle =& \int \mathrm{d}x[\phi_{\mathrm{Ra}}(x)C^\dagger_{\mathrm{Ra}}(x) + \phi_{\mathrm{Lb}}(x)C^\dagger_{\mathrm{Lb}}(x)]|0_a,0_b,0_c,g\rangle \\ &+ \xi_c|0_a,0_b,1,g\rangle + \xi_e|0_a,0_b,0_c,e\rangle \\ &+ \xi_s|0_a,0_b,0_c,s\rangle. \end{aligned} \tag{2}$$

Here, ξ_c denotes the probability amplitude of the excited state of the single-mode whispering gallery resonator, while ξ_e and ξ_s describe the probability amplitudes of the excited state and metastable state of the three-level system, respectively. $\phi_{\mathrm{Ra}}(x)$ $[\phi_{\mathrm{Lb}}(x)]$ is the wave function for the right (left) mode in two waveguides, and their corresponding expressions are given by

$$\begin{aligned} \phi_{\mathrm{Ra}}(x) &= \mathrm{e}^{\mathrm{i}kx}[\theta(-x) + t_a\theta(x)], \\ \phi_{\mathrm{Lb}}(x) &= \mathrm{e}^{-\mathrm{i}kx}t_b\theta(-x). \end{aligned} \tag{3}$$

Here, t_a and t_b represent the transmission and transfer amplitudes in two waveguides, respectively. $\theta(x)$ is the Heaviside step function, with $\theta(0) = 1/2$.

By solving eigen-equation $H|\psi\rangle = \omega|\psi\rangle$, the expressions of t_a and t_b can be obtained as

$$\begin{aligned} t_a &= 1 - \frac{2\mathrm{i}\Gamma_a}{[\Delta\omega + \mathrm{i}\gamma_c + \mathrm{i}(\Gamma_a + \Gamma_b)] - \dfrac{G^2}{\Delta\omega_e + \mathrm{i}\gamma_e - S(\omega)}}, \\ t_b &= \frac{-2\mathrm{i}\sqrt{\Gamma_a\Gamma_b}}{[\Delta\omega + \mathrm{i}\gamma_c + \mathrm{i}(\Gamma_a + \Gamma_b)] - \dfrac{G^2}{\Delta\omega_e + \mathrm{i}\gamma_e - S(\omega)}}, \end{aligned} \tag{4}$$

where $S(\omega) = \Omega^2/(\Delta\omega_s + \mathrm{i}\gamma_s)$ stands for the optical Stark shift. $\Delta\omega = \omega - \omega_c$, $\Delta\omega_e = \omega - \omega_e$, and $\Delta\omega_s = \omega - \omega_s$ describe the frequency detunings for the input photon from the resonator, excited state, and intermediate state, respectively. $\Gamma_a = V_a^2/(2\upsilon_g)$ and $\Gamma_b = V_b^2/(2\upsilon_g)$.

3. Single-photon routing via a coupled single-mode resonator

In the two-waveguide-channel system, the routing characteristics of single photons are governed by the transmission probability $T_{a(b)} = |t_{a(b)}|^2$. As a comparison, we first investigate the bare-resonator case with $G = 0$, in which the three-level system is decoupled from the resonator. When a single photon is input from the left port of the bus waveguide, it will move forward or transfer to the waveguide b through the single-mode resonator. When the dissipations are not included, the photon flow in two ports has conservation relation $T_b + T_a = 1$. Figures 2(a)–2(c) show the transmission flow exchanges between two waveguides for different coupling ratios $P = \Gamma_b/\Gamma_a = 0.5$, 1, 2. As shown in the figure, the routing probability T_b exhibits the maximum value at the resonance point $\Delta\omega = 0$ only for $P = 1$. Certainly, the maximum routing probability is easily obtained by the reduced relationship of $T_b = 4P/(P+1)^2 = 1$ from Eq. (4). Here, all parameters are normalized by Γ_a for simplification. In the ($\Delta\omega$, P) plane in Fig. 2(d), T_b versus more coupling ratios in the frequency

range are further presented. When varying P, a wide elliptical region of high routing rate $T_b \geq 0.9$ is exhibited in the scattering spectra, and a routing peak almost approaching 1 emerges around $P = 1$. The result arises from the fact that two symmetrical transfer paths between the coupled resonator and two waveguides are formed for the equal waveguide–resonator coupling, and thus the routed photon can be completely redirected into the drop waveguide on resonance.

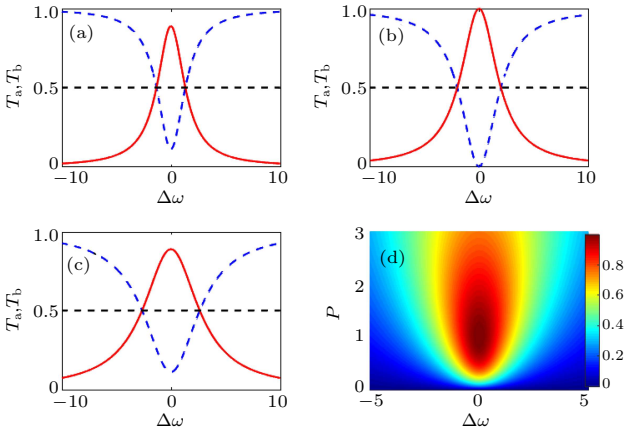


Fig. 2. Transmission T_a (blue dashed curves) in waveguide a and routing rate T_b in waveguide b (red solid curves) versus the detuning $\Delta\omega$. (a) $P = 0.5$, (b) $P = 1$, and (c) $P = 2$. (d) T_b as a function of P and $\Delta\omega$. For convenience, all parameters are in units of Γ_a.

Then we consider the coupled-resonator case for $G \neq 0$ and $P = 1$ in the absence of dissipations. When the classical driving field is tuned off, *i.e.*, $\Omega = 0$, the three-level system is reduced to a two-level qubit. In the case, the routing probability in Eq. (4) can be simplified as

$$T_b = \frac{1}{1 + \dfrac{(\Delta\omega^2 + \Delta\omega\Delta\omega_{ce} - G^2)^2}{4(\Delta\omega + \Delta\omega_{ce})^2}}. \tag{5}$$

As displayed in Figs. 3(a)–3(c), two distinct peaks approaching 100% routing efficiency for T_b and two corresponding zero dips for T_a are exhibited separately at $\Delta\omega = (-\Delta\omega_{ce} \pm \sqrt{\Delta\omega_{ce}^2 + 4G^2})/2$ with a separation of $\sqrt{\Delta\omega_{ce}^2 + 4G^2}$, $\Delta\omega_{ce} = \omega_c - \omega_e$ being the frequency detuning between the resonator and the excited state. In contrast to the above bare-resonator case, it is clear that the single routing channel is switched to the two-resonance mode with two different Rabi-splitting frequencies. Increasing the resonator–qubit coupling G, the routing peak separation becomes wide, and continuous center-frequency locations shift outward approximately linearly in the wide frequency range, as shown in Fig. 3(d). The resonator–qubit coupling strength can be tuned by the their separation and mode polarization of the atomic exciton. For instance, it can be controlled by using an external field to orient the dipole-moment direction of the atomic exciton.[37,39] Consequently, a tunable high-efficiency router can be obtained by varying the coupling.

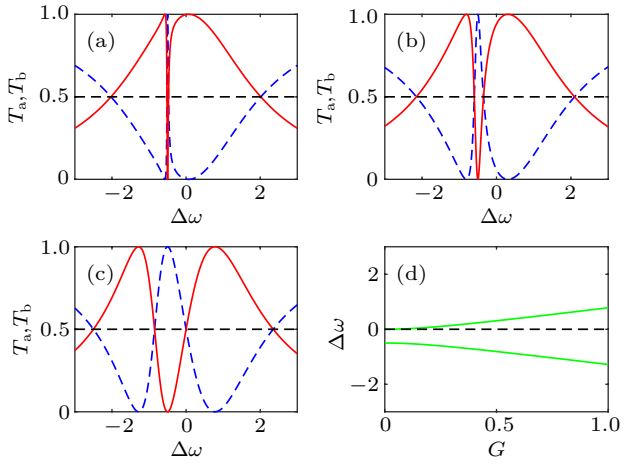


Fig. 3. Transmission T_a (blue dashed curves) and routing rate T_b (red solid curves) for different resonator–qubit couplings: (a) $G = 0.2$, (b) $G = 0.5$, and (c) $G = 1$. Center frequencies of two peaks vary with G in panel (d). The other parameters are $P = 1$ and $\Delta\omega_{ce} = 0.5$.

Further, when the classical field is employed, the three-level system is detuned from the incoming photon by the optical Stark shift $S(\omega)$, which will result in a significant change for the routing properties in the drop waveguide. Similarly, the reduced formula of the routing probability in Eq. (4) is expressed as follows:

$$T_b = \frac{1}{1 + \dfrac{[\Delta\omega(\Delta\omega + \Delta\omega_{ce})(\Delta\omega + \Delta\omega_{cs}) - \Omega^2\Delta\omega - G^2(\Delta\omega + \Delta\omega_{cs})]^2}{4[(\Delta\omega + \Delta\omega_{ce})(\Delta\omega + \Delta\omega_{cs}) - \Omega^2]^2}}. \tag{6}$$

Obviously, there exist three frequency values for the maximum routing rate. As shown in Figs. 4(a)–4(c), three prefect peaks for T_b with wider frequency scope are observed separately at three different resonance points in the scattering spectra. Two bilateral on-resonance peaks also move continuously, and the separation of these two center frequencies broadens with the increase of the drive, with the help of optical Stark shift. Similar to the above case, peak frequency versus the drive is plotted in Fig. 4(d). It shows that three on-resonance frequencies in the drop waveguide emerge, and the middle on-resonance frequency vary slight, while another two frequencies expand sharply in the broad blueshift and redshift frequency ranges, with almost linear relations for the drive. This indicates that the input photons with two movable resonance frequencies are completely routed to the output port, and the frequency-tunable router can also be available by varying the drive.

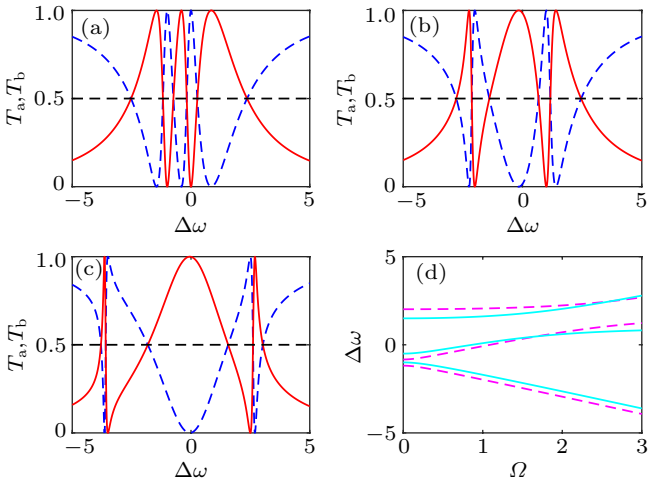


Fig. 4. Transmission T_a (blue dashed curves) and routing rate T_b (red solid curves) for different drives: (a) $\Omega = 0.5$, (b) $\Omega = 1.5$, and (c) $\Omega = 3$, and $\Delta\omega_0 = 0.5$. Center frequencies of three routing peaks vary with Ω in panel (d), $\Delta\omega_0 = 1.5$ for solid curves and $\Delta\omega_0 = 2.5$ for dashed curves. Here, $\omega_c - \omega_s = \Delta\omega_{cs} = \Delta\omega_{ce} = \Delta\omega_0$ is set. The other parameters are $G = 1$, and $P = 1$.

To gain a deeper insight into the dependence of the photon routing capability on the waveguide–qubit coupling, figure 5 displays routing features in the $(P, \Delta\omega)$ planes for the transfer T_b. Obviously, two wide elliptical region with high routing rate $T_b > 0.9$ are presented in the scattering spectra in Fig. 5(a) for the coupled-qubit case, while three elliptical windows of high routing rates are exhibited when the drive is included in Fig. 5(b). These asymmetrical peaks emerge at their corresponding resonance-frequency locations with the equal coupling ratio $P = 1$, since these propagating photons in the bus waveguide is completely blocked and routed to another waveguide through the symmetrical coupling channels.

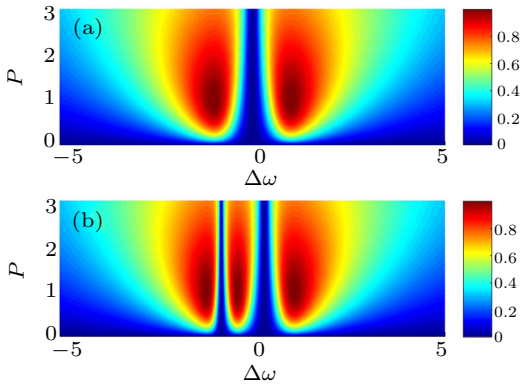


Fig. 5. T_b as a function of the detuning $\Delta\omega$ and the coupling ratio P for (a) $\Omega = 0$ and (b) $\Omega = 0.5$. The other parameters are $G = 1$, $P = 1$, and $\Delta\omega_0 = 0.5$.

Similarly, we also examine the influence of the control field on the resonance frequencies of routing peaks. T_b versus different drives is presented in the $(\Omega, \Delta\omega)$ plane in Fig. 6. When the drive is small, only two asymmetrical peaks occur. When increasing the drive, two peaks move rapidly along a red V-type track, while the middle peak appears and extends slowly. Thus, tunable red-shift and blue-shift resonance frequencies are available for the router by adjusting the driving field of the three-level system.

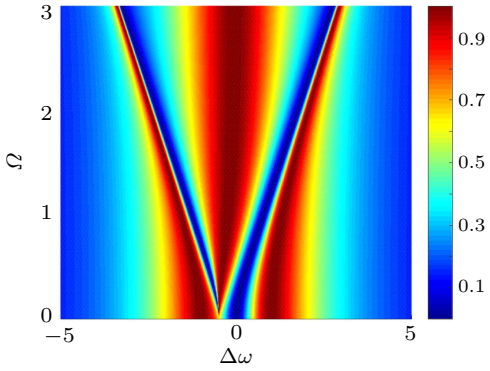


Fig. 6. T_b as a function of the detuning $\Delta\omega$ and the drive Ω. These parameters are the same as those in Fig. 5.

It is worth noting the dissipations are not considered in the above investigations. In fact, the coupled system inevitably suffers dissipations, such as atomic excited-state relaxation and photon leakage of the resonator. Compared to the routing spectra with no dissipations, the routing rates decrease when increasing the dissipations, as shown in Fig. 7(a). For a high-quality resonator with very low losses, however, it is available for high routing efficiency, such as $T_b \approx 0.85$ of one side peak at $\gamma_0 = 0.15$. In addition, figure 7(b) displays the influence of the resonator–waveguide coupling on the routing T_b at the middle resonance frequency $\Delta\omega = -0.16$. For low dissipation ($\gamma_0 = \Gamma_a/20$), high routing peak occurs with the equal coupling around $P = 1$. While for high dissipation ($\gamma_0 = \Gamma_a$), routing peak fall sharply, and shifts to a big value about $P = 2$, since photon transfer reduces due to the photon leakage and stronger coupling Γ_b is expected to enhance the transfer to the drop waveguide.

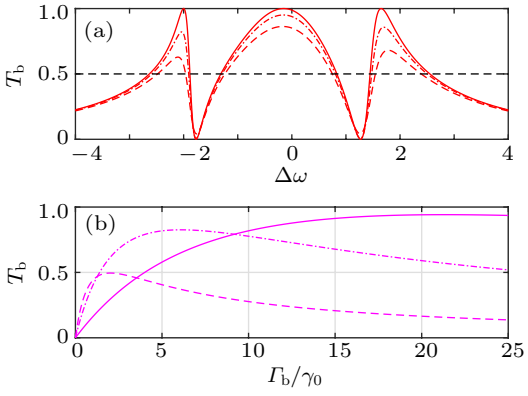


Fig. 7. (a) T_b for different dissipations: zero dissipations (solid line), $\gamma_0 = \gamma_c = \gamma_e = 10\gamma_s = 0.15$ (dash dotted line), and $\gamma_0 = 0.2$ (dashed line). (b) T_b at the middle center frequency $\Delta\omega = -0.16$ for different coupling-dissipation ratio Γ_b/γ_0 at $\Omega = 1.5$ (solid line for $\Gamma_a/\gamma_0 = 20$, dash dotted line for $\Gamma_a/\gamma_0 = 5$, and dashed line for $\Gamma_a/\gamma_0 = 1$). Other parameters are $G = 1$, $P = 1$, $\Delta\omega_{ce} = 0$, and $\Delta\omega_{cs} = 0.5$.

4. Conclusion

In summary, we have investigated the frequency-tunable routing of single photons in a waveguide–resonator system

with a driven three-level emitter. By a full quantum approach, the photon routing probability transferring to the output port is obtained exactly, and some frequency of the routing photon can be effectively manipulated on demand, with the good tunability for the driving pump. Note that the routing photon moves out in the left port of the drop waveguide, via the mode matching of the guided-wave mode and resonator mode. Another port can be open to get two-port routing when adding an clockwise-mode resonator system and a rearmounted reflector, with a suitable inter-resonator detuning to suppress their crosstalk. Therefore, such proposed routers have wide potentials in frequency-modulation quantum information.

Acknowledgements

Project supported by the National Natural Science Foundation of China (Grant Nos. 12365003, 12364024, and 11864014) and the Natural Science Foundation of Jiangxi Province, China (Grant Nos. 20212BAB201014 and 20224BAB201023).

References

[1] Kimble H J 2008 *Nature* **453** 1023
[2] Goban A, Hung C L, Yu S P, Hood J D, Muniz J A, Lee J H, Martin M J, McClung A C, Choi K S, Chang D E, Painter O and Kimble H J 2014 *Nat. Commun.* **5** 3808
[3] Shomroni I, Rosenblum S, Lovsky Y, Brechler O, Guendelman G and Dayan B 2014 *Science* **345** 903
[4] Li X M and Wei L F 2015 *Phys. Rev. A* **92** 063836
[5] Huang J S, Zhong J T, Li Y L, Xu Z H and Xiao Q S 2020 *Quantum Inf. Process.* **19** 290
[6] Wu J N, Dong J, Xu Y, Zou B and Zhang Y 2022 *Phys. Rev. Appl.* **18** 054007
[7] Zhao Y J, Tan N, Yu D, Liu B and Liu W M 2020 *Phys. Rev. Res.* **2** 033484
[8] Hoi I C, Wilson C M, Johansson G, Palomaki T, Peropadre B and Delsing P 2011 *Phys. Rev. Lett.* **107** 073601
[9] Xia K and Twamley J 2013 *Phys. Rev. X* **3** 031013
[10] Zhou L, Yang L P, Li Y and Sun C P 2013 *Phys. Rev. Lett.* **111** 103604
[11] Lu J, Wang Z H and Zhou L 2015 *Opt. Express* **23** 022955
[12] Huang J S, Wang J W, Li Y L, Wang Y and Huang Y W 2019 *Quantum Inf. Process.* **18** 59
[13] Hu C Y 2016 *Phys. Rev. B* **94** 245307
[14] Hu C Y 2017 *Sci. Rep.* **7** 45582
[15] Agarwal G S and Huang S 2012 *Phys. Rev. A* **85** 021801
[16] Li X, Zhang W Z, Xiong B and Zhou L 2016 *Sci. Rep.* **6** 39343
[17] Aoki T, Parkins A S, Alton D J, Regal C A, Dayan B, Ostby E, Vahala K J and Kimble H J 2009 *Phys. Rev. Lett.* **102** 083601
[18] Cao C, Duan Y W, Chen X, Zhang R, Wang T J and Wang C 2017 *Opt. Express* **25** 016931
[19] Huang J S, Wang J W, Wang Y, Li Y L and Huang Y W 2018 *Quantum Inf. Process.* **17** 78
[20] Zhang J H, He D Y, Luo G Y, Wang B D and Huang J S 2021 *Chin. Phys. B* **30** 034204
[21] Gonzalez-Ballestero C, Moreno E, Garcia-Vidal F J and Tudela A G 2016 *Phys. Rev. A* **94** 063817
[22] Yan C H, Li Y, Yuan H D and Wei L F 2018 *Phys. Rev. A* **97** 023821
[23] Li X M and Wei L F 2018 *Opt. Commun.* **425** 13
[24] Liu J S, Yang Y, Lu J and Zhou L 2022 *Chin. Phys. B* **31** 110301
[25] Sun X J, Liu W X, Chen H and Li H R 2023 *Commun. Theor. Phys.* **75** 035103
[26] Del'Haye P, Herr T, Gavartin E, Gorodetsky M L, Holzwarth R and Kippenberg T J 2011 *Phys. Rev. Lett.* **107** 063901
[27] Miller S A, Okawachi Y, Ramelow S, Luke K, Dutt A, Farsi A, Gaeta A L and Lipson M 2015 *Opt. Express* **23** 021527
[28] Cai G Q, Lu Y N, Ma X S, Cheng M T and Huang X S 2023 *Opt. Express* **31** 33015
[29] Khani S, Danaie M and Rezaei P 2018 *Opt. Commun.* **420** 147
[30] Khani S, Danaie M and Rezaei P 2019 *Plasmonics* **14** 53
[31] Ren L, Yuan S, Zhu S, Shi L, Zhang X 2022 *Opt. Lett.* **47** 468442
[32] Zhang B W, Chen N, Lu X D, Hu Y H, Yang Z H, Zhang X L and Xu J 2022 *Micromachines* **13** 89
[33] Tian M E, Long Z H, Feng L J, He L L and Zhang T L 2022 *Chin. Phys. B* **31** 078401
[34] Zhang X W, Liu S B, Yu Q M, Wang L L, Liao K and Lou J 2022 *Chin. Phys. B* **31** 114101
[35] Han L L, Wang Y, Wu Q, Zhang S, Wang S and Li M 2022 *Chin. Phys. B* **31** 018506
[36] Huang J S, Feng X M, Xu Z H, Li Y L and Wu K Y 2023 *Quantum Inf. Process.* **22** 285
[37] Shen J T and Fan S H 2009 *Phys. Rev. A* **79** 023837
[38] Witthaut D and Sørensen A S 2010 *New J. Phys.* **12** 043052
[39] Srinivasan K and Painter O 2007 *Phys. Rev. A* **75** 023814